ARTICLES

nature neuroscience

Rapid global shifts in natural scenes block spiking in specific ganglion cell types

Botond Roska[1–3] & Frank Werblin[1]

The mammalian retina contains more than a dozen different ganglion cell types, each with dendrites ramifying at different strata within the inner plexiform layer (IPL) and each carrying a unique representation of the visual world. We studied the inhibitory and excitatory inputs, as well as the spiking output, of each of the rabbit retinal ganglion cell type during rapid global shifts in 'natural' videos designed to mimic saccadic eye movements. These shifts generated stratum-specific transient inhibitory activity, affecting only those ganglion cells whose dendrites ramify within the central strata of the IPL. The inhibition was GABA-mediated, acted both pre- and postsynaptically and was fast enough to either prevent or delay spiking. These findings indicate that the fast, transient elevation of visual threshold during rapid shifts in scene has a significant retinal component.

The vertebrate retina achieves its most sophisticated level of processing at the inner plexiform layer, where ten different bipolar inputs[1–4], modulated by as many as 28 different amacrine cell interneurons[5], organize the parallel processing[6–8] of at least ten different ganglion cell types in a variety of species: cat[9], rabbit[6,10,11], mouse[12], rat[13], guinea pig (P. Sterling, Univ. of Pennsylvania, personal communication), primate[14,15], zebrafish[16], mudpuppy[17] and frog[18]. Each of these ganglion cell types locally integrates spatially and temporally different inhibitory and excitatory inputs[6,19] to form at least ten parallel neural representations of the visual world[6] in well-defined anatomical strata.

These local representations are themselves subject to modulation by more spatially extensive, or 'global,' retinal circuitry: global image movements that naturally occur during saccadic eye movements activate both inhibitory[20–25] and excitatory lateral[26–31] pathways. In salamanders, global movement evoked by a spinning windmill[20,21,24,25], activates large field spiking in glycinergic amacrine cells, which in turn inhibit transient ON-OFF ganglion cells. In mammals, global visual stimulation results in both excitation and inhibition. In cat retinal Y ganglion cells, sudden displacement of a pattern far away from the receptive field center elicits a transient excitatory response, or 'shift effect'[26–28,30,31]. Stimulation of the same area also results, however, in amacrine-mediated inhibition of ganglion cells[22,23,32,33].

How are inhibition and excitation during global shifts integrated in different ganglion cell types in the mammalian retina?

To address this question, we investigated how local interactions in each ganglion cell type in the rabbit retina are affected by global inhibition and excitation elicited by abrupt spatial shifts in videos (**Supplementary Fig. 1** online). See **Supplementary Video** online for an example (video I); the rest of the videos can be viewed at http://mcb.berkeley.edu/labs/werblin/. We found that certain ganglion cell types were transiently suppressed at scene shifts and scene cuts of naturalistic videos. This suppression was brought about in specific strata by a rapid inhibitory input that was faster than excitation and therefore able to suppress initial spiking. This rapid inhibitory input could be evoked by other spatially global and transient forms of illumination, such as a checkerboard.

RESULTS

We found five ganglion cell types in which rapid, global shifts suppressed or delayed spiking output. For these suppressed cell types, the shift elicited a transient, fast inhibitory event that was coincident at every spatial location within the bounds of the video (**Fig. 1a**,**b**, $n = 16$). A similar temporally coincident inhibition was measured at scene cuts (**Fig. 1d**, second transient) or when the video was started and stopped (**Fig. 1b**,**c**). During the shift, spiking was reduced (**Figs. 1c** and **2**), probably because inhibition suppressed excitation. At the time of the rapid shift, large excitatory currents at some locations did not elicit spiking, yet at other times, much smaller currents could elicit spiking (compare excitation and spiking at arrows 1 and 2 in **Fig. 1c**). In contrast to abrupt image shifts, fast but sustained image movement did not cause significant inhibition (**Fig. 1d**). The lack of large inhibitory input during the sustained shift cannot be explained by image blur because the excitatory input and spiking of type-5/6 cells, for example, faithfully followed the moving contrast borders of the shifting scene (**Fig. 1e**). These results suggest that transient, spatially extensive changes of scene initiate a widespread inhibition that reduces spiking in all suppressed cell classes.

Two of the five suppressed cell types (type 4 and type 5/6) often spiked near the time of the shift (**Fig. 2**), but this spike burst was delayed by an earlier onset of inhibition so that spikes appeared later than the onset of the excitatory input. When the five suppressed cell classes were tested with light flashes of different sizes (50–2,000 μm; **Fig. 2e**), the inhibitory response to a large spot (1,000–2,000 μm) was faster than the fastest excitatory input (Methods). Most suppressed cells had dendritic diameters of less than 350 μm.

[1]Department of Molecular and Cell Biology, University of California Berkeley, 145 LSA, California 94720, USA. [2]Department of Medical Biochemistry, Semmelweis University, Puskin utca 9, Budapest 1088, Hungary. [3]Present address: Harvard Society of Fellows, Harvard University, 78 Mount Auburn Street, Cambridge, Massachusetts 02138, USA. Correspondence should be addressed to B.R. (roska@fas.harvard.edu).

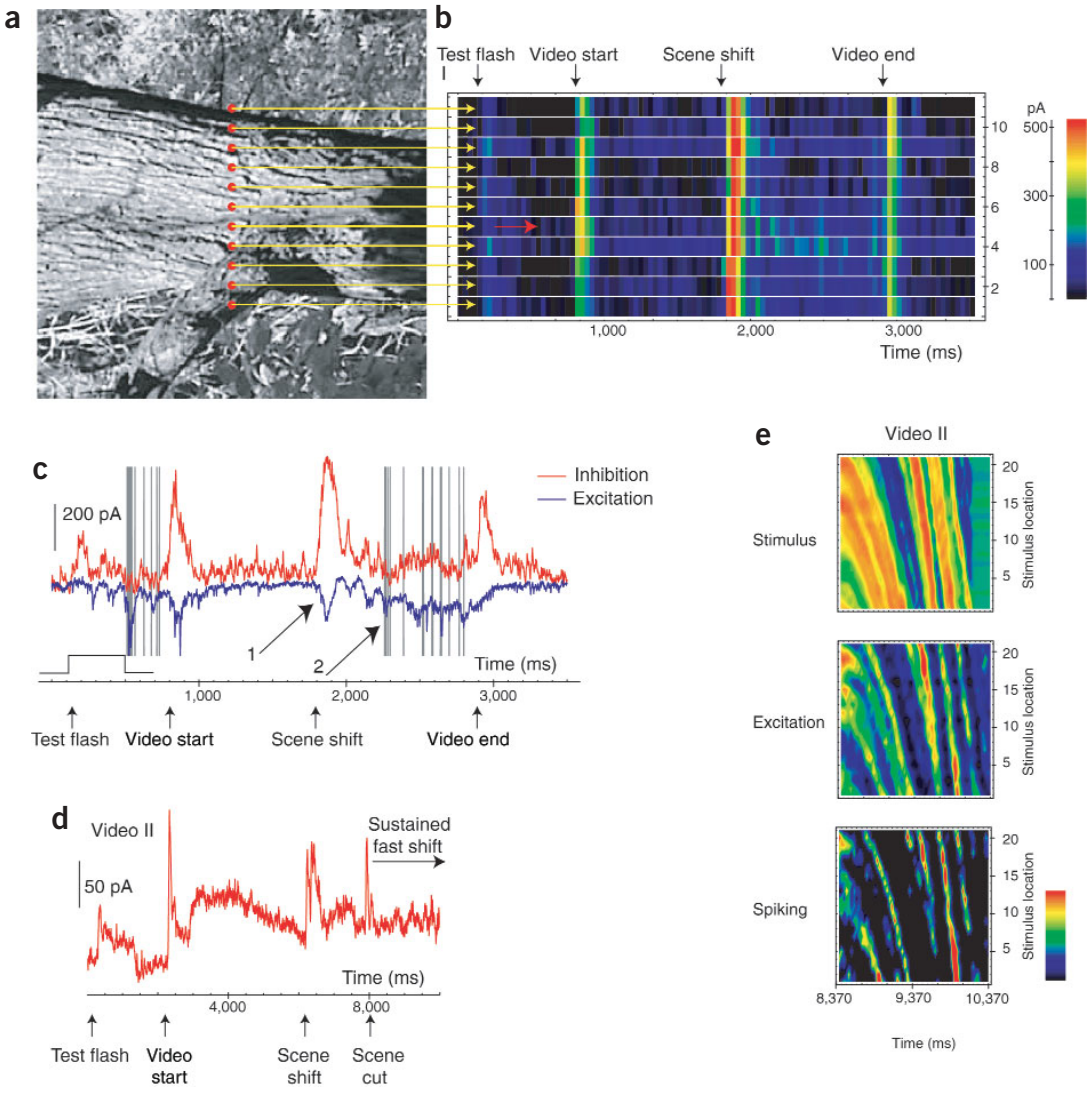

Figure 1 Global scene shifts elicit inhibition. (**a**) The first frame of a video (30 frames/s) rotated by 90°. Red dots show the locations of the electrode on this projected video for each of the 11 separate presentations. The frame is rotated in this figure to simplify the connection between panels **a** and **b**. (**b**) Time course of inhibitory current responses, measured from each electrode location under whole-cell voltage clamp at 0 mV. The different current magnitudes were converted into different colors according to the current-to-color map shown on the right (red, maximum inhibition; black, no inhibition) and displayed in each of the 11 rows. The plot shows non-averaged records. (**c**) Inhibition (red), excitation (blue) and spikes (black lines) measured at location 5 (red arrow in **b**). Arrow 1 points to an excitatory event during a scene shift that does not evoke spikes; arrow 2 points to a smaller excitatory event after the shift that evokes spikes. Before each video presentation, we tested the response of the measured cell with a 100-µm diameter white spot (test flash). This cell was an OFF ganglion cell, so it spiked when the spot was turned off at 500 ms. This spot test ensured that the response properties of the measured cell did not change during the experiments. (**d**) Inhibition during a video presentation. First global event, scene shift; second global event, scene cut. The last part of the video was a sustained fast shift (4.25 mm/s imaged on the retina, 25° of visual angle/s) in the scene. (**e**) The color-coded stimulus (top), measured with a photodiode, and the excitatory (middle) and spiking (bottom) patterns measured at 21 locations separated by 50 µm (Methods) during the sustained shift in **d** (video II) from type-6 cells. The color code is shown on the right (black, low activity; red, high activity). The roman numbers on each figure refer to different stimulus videos (see Methods).

In five other ganglion cell classes, spiking was not suppressed by abrupt shifts (**Fig. 3**). In fact, three of them actively burst during the scene shift (**Fig. 3f**). In those cell types, the inhibition measured at the time of the shift lagged behind the excitatory input. In each of these non-suppressed cell classes, even the fastest inhibitory component in response to a large test spot was slower than the excitatory input (**Fig. 3e**).

The dendritic trees of suppressed cells all ramified within two bands of the inner plexiform layer formed by the dendrites of directionally selective ganglion cells, but those of the non-suppressed cell classes coincided with or fell outside those bands (**Fig. 4**). This suggests that the processes of those amacrine cells that provide the shift-elicited fast inhibition for the suppressed cells also ramify within these bands.

The transient global inhibition associated with the shift can be obscured by ongoing local inhibition. **Fig. 5a** shows a set of inhibitory current traces elicited by a shift in an OFF ganglion cell centered in seven different videos ($n = 8$). In five of the seven videos, the transient shift inhibition is obvious. But in presentations 2 and 5, an ongoing inhibition, already present before the shift, obscured the shift-elicited inhibition. To eliminate this ongoing inhibitory component, we

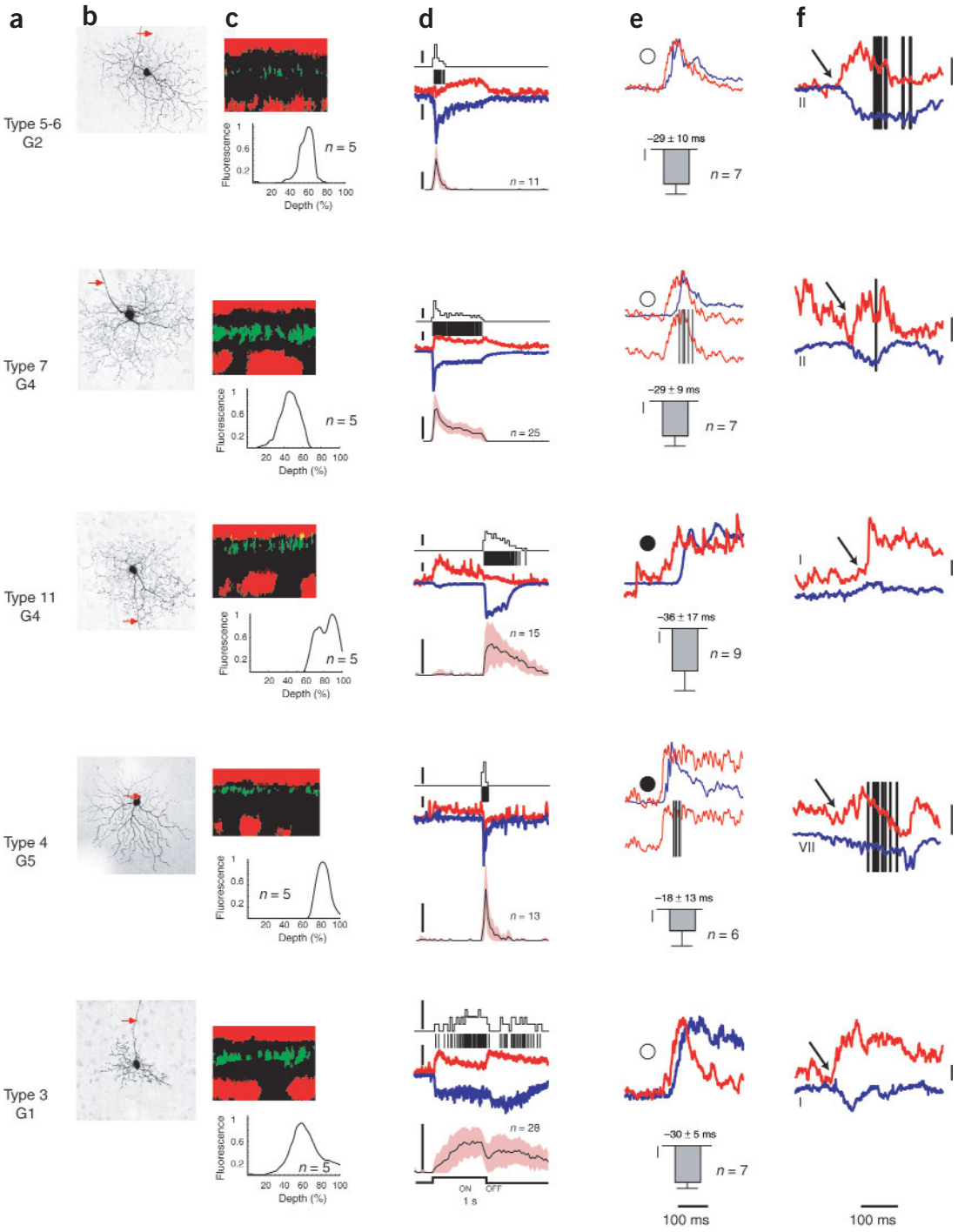

Figure 2 Parallel processing of global image shifts: suppressed cell types. For each cell type, an individual example is shown above, the group data below. (**a**) The names of the ganglion cell types[6] and their G1–11 classification[10]. (**b**) Top view of the different ganglion cell types from confocal reconstructions. The red arrows point to the axons. (**c**) Above, depths of dendritic ramifications (cell bodies, red; measured ganglion cell dendrites, green; top, distal retina; bottom, proximal retina). Below, the average dendritic ramification measured from five cells in each class. (**d**) Above, excitatory (blue), inhibitory (red), spiking (black) and binned spiking (bin window, 50 ms) responses to a 100-μm white spot flashed for 1 s. Vertical scale bars, 100 pA for the currents and 100 spikes/s for the spike frequency. Below, the mean spike frequency responses to the flash from many cells of the same type. The pink area shows the standard deviation in time. (**e**) Above, the fastest (see Methods) excitatory response (blue, current is reversed for comparison) and the inhibitory response (red) to a 1,000–2,000 μm spot flashed for 1 s. The polarity (black or white circle) of the spots is indicated on the left. The response amplitude is normalized to the maximum of the light-evoked current. Only the response onset is shown. When the cell showed a spiking response to the 1,000-μm spot, it was also plotted together with the inhibition. Note that the spiking is shown to a 1,000-μm spot, whereas the excitatory response shown is the fastest measured response to different sized spots. Lower red trace is the mean ± s.d. of the difference in time between the onset of the fastest excitation and the onset of the global inhibition for each cell type. The onset of the current was defined as the time when the current reached 50% of the peak. Note that in type-9 cells, the magnitude of the inhibitory response was one-tenth of the excitatory response at light ON. (**f**) Excitatory (blue), inhibitory (red) and spiking (black) responses to a shift in a natural video. The black arrows indicate the start of the shift. Vertical bars at right, 100 pA.

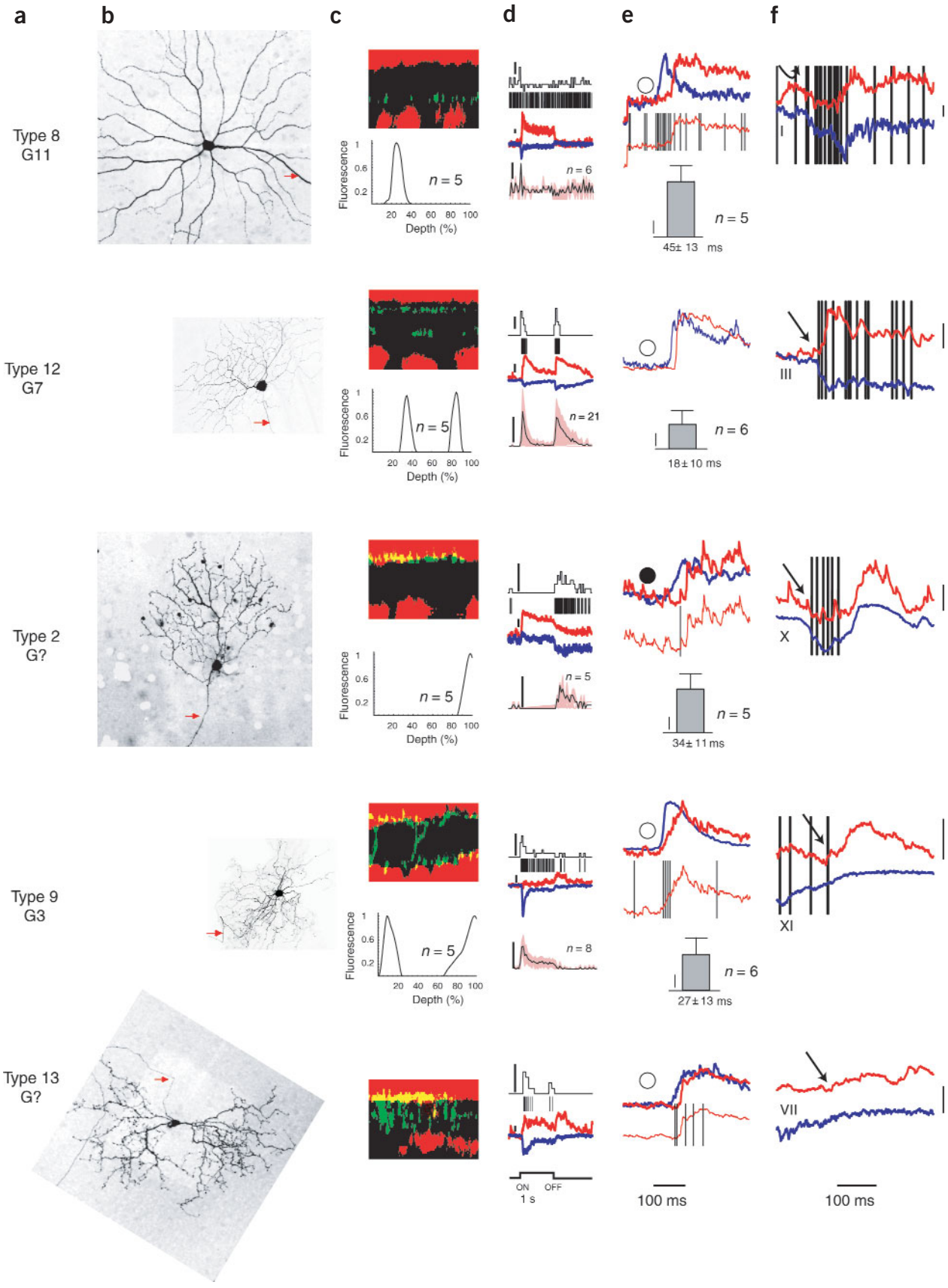

Figure 3 Parallel processing of global image shifts: non-suppressed cell types. See **Fig. 2** legend.

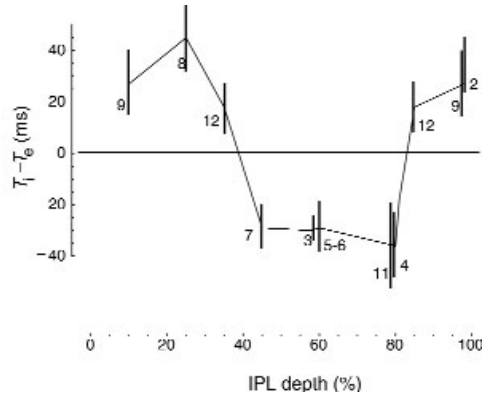

Figure 4 The dendritic stratification of suppressed and non-suppressed cells in the IPL. The time difference between the onset of the 1,000 µm spot evoked inhibition (T_i) and the fastest excitation (T_e, data from **Figs. 2** and **3e**) is plotted as a function of the depth of dendritic ramification (data from **Figs. 2** and **3c**, the depth of dendritic ramification is defined to be the depth at the peak of fluorescence) for each cell class. Red bars show the standard deviation (s.d.). The cell types are noted next to each bar. 0% defines the border between the ganglion cell layer and IPL.

masked (n = 11) the central part of the video with a 700–1,000 µm diameter gray disk so that no intensity change occurred in the vicinity of the recorded cells during the video. In the presence of the mask, inhibition decreased significantly throughout the measurement except at the time of the shift (**Fig. 5b**). The mask therefore isolated the inhibitory component that was specifically activated by the shift in the video. This shows that rapid shift-evoked inhibition can be initiated from a distance and therefore would be active even in the presence of large, uniform objects in the scene.

Abrupt scene shifts can lead to excitatory activity (shift effect[27]) in the presence of a mask. This shift effect arose in two suppressed cell types that often showed a delayed burst during a shift (type 5/6 and type 4), as well as in non-suppressed cell types. We uncovered two novel features (**Fig. 5c**) of the shift effect. First, both the timing (compare columns 2 and 3 in **Fig. 5c**) and the magnitude (compare columns 1 and 2 in **Fig. 5c**) of the shift effect were strongly dependent on the specific video. Second, the shift effect was completely absent in natural videos without a mask and only appeared when an artificial gray mask covered the dendritic field of the measured cell (**Fig. 5c**, column 3). Because the shift effect is not always apparent under natural conditions, it is not likely to carry an unambiguous shift-related signal[31] to higher visual centers.

The non-suppressed cell types behaved in two different ways in the presence of the central mask (**Fig. 5d**). In type-8 cells, inhibition simply disappeared when the central part of the video was masked, suggesting that inhibition was generated locally. In the other non-suppressed cells, a delayed inhibition persisted during the mask, suggesting a global source of inhibition but with a slower time course.

In suppressed cells, the magnitude and waveform of inhibition was similar at every location under a shifting scene (**Fig. 6a**, upper row). This inhibition did not depend on the magnitude and waveform of local illumination at the measured ganglion cell (**Fig. 6a**, lower row), as also suggested by the mask experiments. For example in **Fig. 6a**, inhibition at

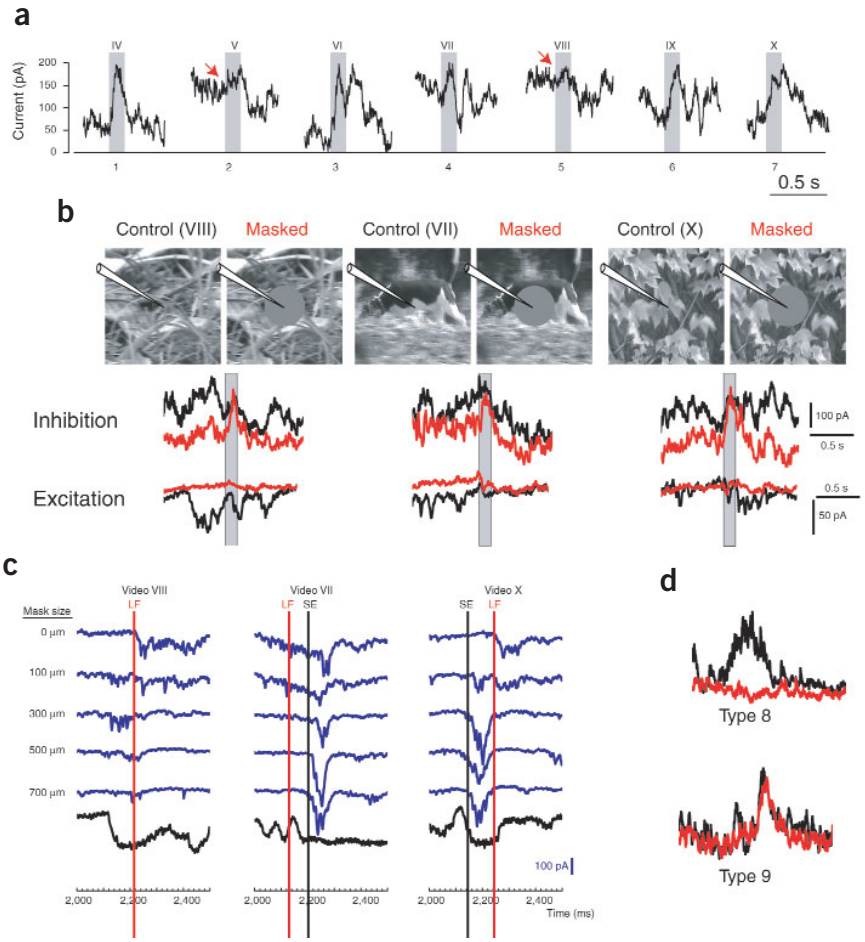

Figure 5 Isolating the shift inhibition. (**a**) Inhibition measured at the center of the video from a suppressed cell during the presentations of seven different videos (indicated by roman numerals). The gray bars show the timing of the shift. (**b**) The first frame of three different videos with and without a 700-µm mask is shown above with the location of the electrode. The inhibitory and excitatory currents during a part of the video presentations, encompassing the shift, are shown below. Red traces, responses with mask; black traces, responses without mask. The gray bars show the timing of the shift. (**c**) Excitatory currents (blue) from cell type 4 during three different video presentations shown in each of the three columns. The videos are the same as in **b**. Each row shows responses at different mask sizes covering the central part of the video. The change of illumination measured with a photodiode centered at the measured cell during the video (without a mask) is shown in black in the bottom row. Red lines show the timing of local visual feature induced excitatory currents (LF) that disappear with large masks. Black lines show the timing of global visual feature–induced excitatory currents (shift effect, SE) that are preserved at large mask sizes. The gray bars show the timing of the shift. (**d**) Inhibition with (red) or without (black) a 700-µm mask in non-suppressed cells.

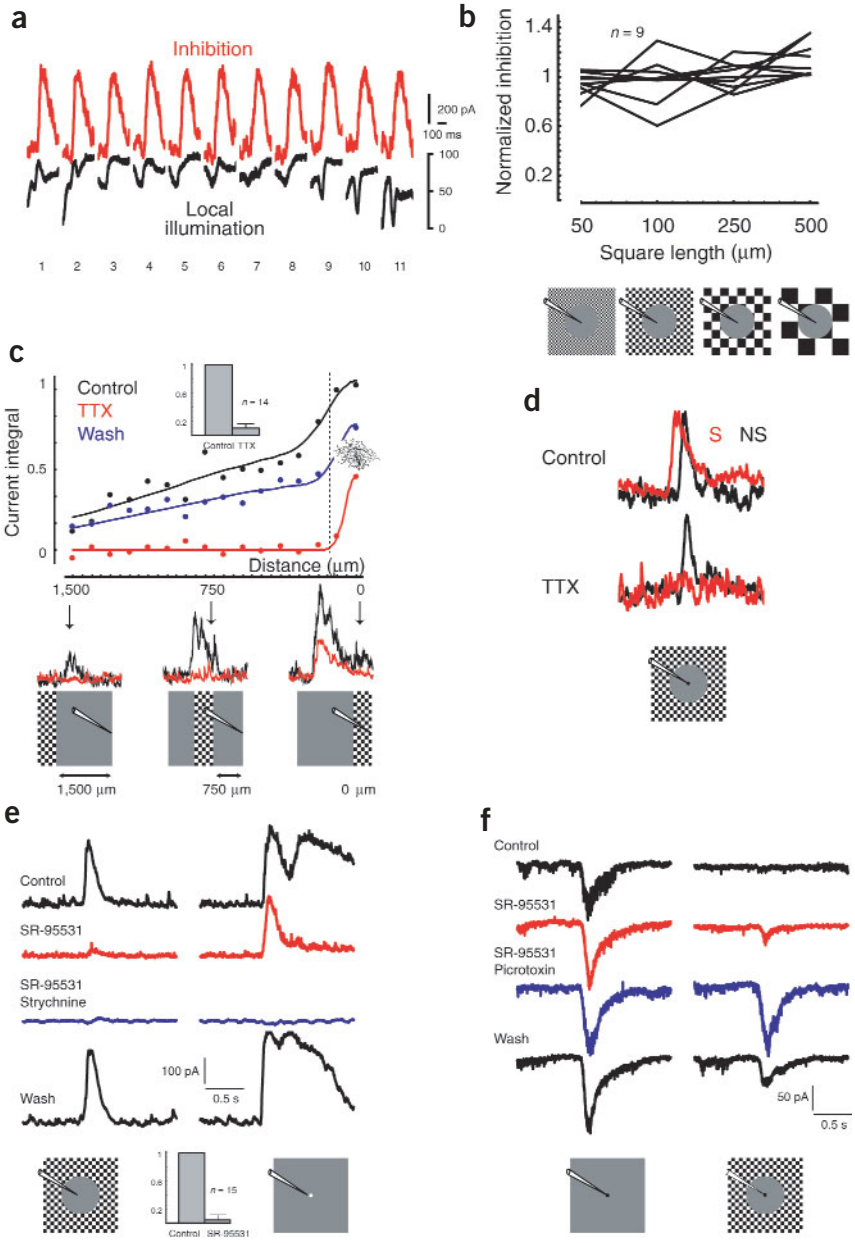

Figure 6 Properties of the fast inhibition to suppressed cells. (**a**) The shape and magnitude of inhibition at 11 locations under the same video (red traces) and the local illumination during a shift (black traces). (**b**) The integral of the inhibitory current evoked by checkerboard flickers outside a 1,000-μm mask (normalized to the mean current integral evoked by different size checkerboards) is plotted as a function of the size of the squares in the checkerboard. Each of the nine curves is measured from a different suppressed cell. (**c**) The integral of the inhibitory current (normalized to the largest evoked current integral in the control measurement) evoked by a checkerboard stripe flicker is plotted as a function of distance from a measured cell body. Black trace, control; red trace, 1 μM TTX; blue trace, wash. The confocal reconstruction of the dendritic tree of the measured cell indicates the size of the dendrites. The dashed line shows the border of the dendrites. The three curves below the graph show responses with (red) and without TTX (black) at three different distances (1,500, 700 and 0 μm). The inset shows the average reduction of inhibitory currents by 1 μM TTX evoked by a checkerboard stripe flicker 1,000 μm from the measured cell. (**d**) The effect of TTX (lower curves) to the flicker inhibition in a suppressed (red curve) and a non-suppressed (black curve) cell. (**e**) Inhibitory responses to a checkerboard flicker around a 1,000 μm mask (left column) and to a spot (right column). Upper black trace, control; red trace, 5 μM SR-95531; blue trace, 5 μM SR-95531 and 10 μM strychnine; lower black trace, wash. The inset shows the average reduction of transient flicker inhibitory currents by 5 μM SR-95531. (**f**) Excitatory responses to a spot (left column) and to a spot and a checkerboard flicker around a 1,000-μm mask (right column). Upper black trace, control; red trace, 5 μM SR-95531; blue trace, 5 μM SR-95531 and 100 μM picrotoxin; lower black trace, wash.

locations 2 and 7 are nearly identical, even though the local change of illumination at location 2 was much greater than at location 7.

The inhibition measured during rapid scene shifts does not depend on the spatial details of the scene during the shift. To quantify this idea, we presented a black-and-white checkerboard flicker of different spatial frequencies for 100 ms outside a 1,000 μm diameter mask. **Fig. 6b** shows that the size of the inhibitory transient measured from suppressed ganglion cells at the center of the circular mask ($n = 9$) did not depend on the size of the squares in the checkerboard.

Given that the mask could isolate the shift inhibitory component and that the magnitude of inhibition was independent of the spatial frequency of the checkerboard, we designed a 'general' stimulus consisting of a 1,000-μm gray mask on a black and white checkerboard flicker of 100-μm squares. We used this stimulus to study the pharmacology underlying global-shift inhibition.

The fast inhibition in suppressed cells can be evoked from as far away as 1.5 mm from the measured ganglion cell, and it can be blocked by tetrodotoxin (TTX; $n = 14$)[21,32], suggesting that lateral transmission of this inhibition is carried by propagated sodium spikes (**Fig. 6c**). In non-suppressed cell types where the mask did not block inhibition, TTX had no effect, suggesting that in these cell types, sodium spike propagation is not involved in lateral inhibition (**Fig. 6d**). This finding also might explain why inhibition is slower in these cell types.

The amacrine-to-ganglion cell, fast inhibitory effect could be blocked by the $GABA_A$ receptor blocker SR-95531 (5 μM, $n = 15$; **Fig. 6e**). In the presence of SR-95531, at least one component of the local inhibitory input remained intact in all measured cells. This local inhibitory component was blocked completely by the glycinergic blocker strychnine (10 μM, $n = 8$, **Fig. 6e**). Thus, global inhibition is GABA-mediated, whereas a major component of local inhibition is glycine-mediated[34]. In a subset of suppressed ganglion cells, we found that an excitatory response, evoked by a flashed 100-μm spot, could be decreased by simultaneously presenting the transient flicker. The flicker effect on excitation could not be blocked by SR-95531, but additional $GABA_C$ receptor blockade[35] by picrotoxin (100 μM, $n = 5$) eliminated the flicker-elicited reduction in excitation (**Fig. 6f**). Because $GABA_C$

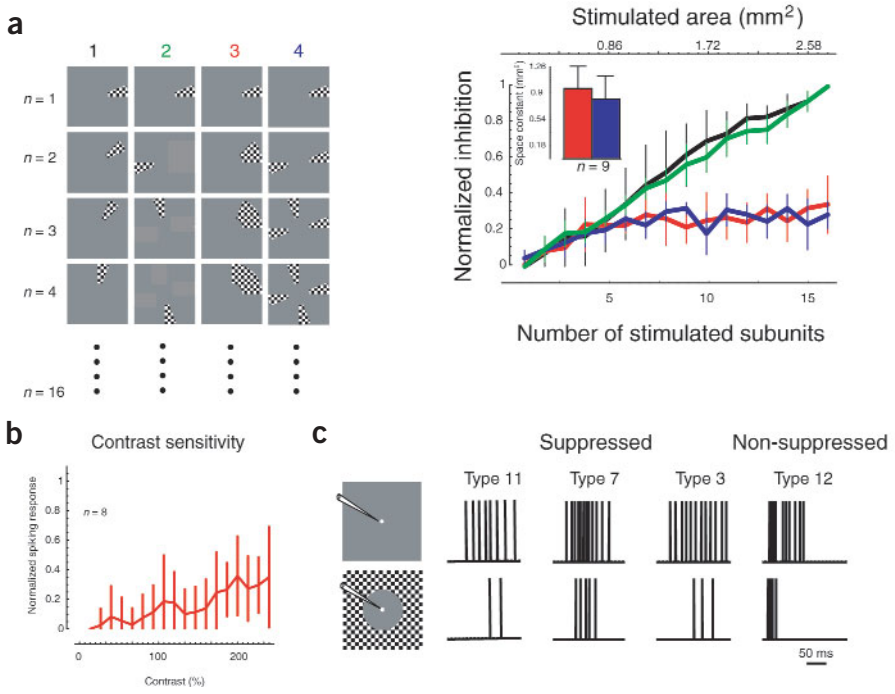

Figure 7 Spatial summation of the global change–evoked inhibition. (**a**) Left, four different experiments are shown. First column, separate flicker stimulation of individual annular segments (1/16 of a ring, 700 μm inner, 2,000 μm outer diameter) around the ganglion cell, 16 separate trials. Second column, separate stimulation of individual annular subregions in a different order. Third column, simultaneous stimulation of an increasing number of contiguous subregions. Fourth column, simultaneous stimulation of an increasing number of disparate subregions corresponding to the subregion order in the second column. Right, black and green traces show the magnitude of the sum of inhibitory currents corresponding to experiments 1 and 2. The number of stimulated sub-regions is shown on the *x*-axis. Red and blue traces show the magnitude of the inhibitory currents corresponding to experiments 3 and 4. All curves were normalized to the magnitude of inhibition evoked by a full flicker ring stimulation. Inset, space constants of the red and blue curves after exponential fitting. (**b**) The effect of flicker stimulation on the spiking response to spots of different contrasts. The *y*-axis shows the number of spikes evoked by simultaneous spot + flicker stimulation at each contrast level (*x*-axis) divided by the number of spikes evoked by spot stimulation only. (**c**) Examples of spiking responses to spot or spot + flicker stimulations at 200% spot contrast in suppressed cells and in a non-suppressed cell.

receptors are concentrated at the bipolar terminals, this suggests that a component of global inhibition is fed back to bipolar cells. Thus, GABA appears to mediate the fast global inhibition, both through a feedforward influence on ganglion cells and feedback influence on bipolar cells.

To understand how globally initiated inhibition is integrated over different spatial regions, we separately or simultaneously stimulated concentrically arranged, annular subregions (subregion area, 0.172 mm^2) with a checkerboard flicker around a central mask. **Fig. 7a** shows that the magnitude of inhibition increased nonlinearly as we stimulated larger and larger annular areas, saturating at around 0.9 mm^2 ($n = 9$), whether or not the stimulated areas were contiguous. If inhibition arrives via independent neural elements, the separate current components should be additive at the ganglion cell membrane. The measured saturation suggests that the neural elements that provide the inhibition are not independent. This is consistent with electrical coupling between the presynaptic inhibitory neurons.

Finally, to further analyze the effect of the inhibition on the spiking output of different ganglion cell types, we stimulated suppressed and non-suppressed ganglion cell types with a 100-μm spot of different contrasts with or without a transient flicker. **Fig. 7b** shows that at all contrast levels, the spiking response to the spot was decreased significantly. At low contrast levels, the response to a spot was completely suppressed, but at higher contrast levels, some spikes could be evoked even in the presence of the transient flicker in suppressed cell classes. In those cases, transient flicker stimulations always caused a delay of spiking at the beginning of spot stimulation (**Fig. 7c**), as suggested by the earlier onset of the shift inhibition (**Figs. 2d** and **6d**). Conversely, in non-suppressed cells (type 12), spiking was truncated only after a delay (**Fig. 7**).

DISCUSSION

Many of the properties of the fast shift inhibition are consistent with the functional properties of the three ON-OFF subtypes of polyaxonal[36–40] amacrine cells. The global shift–induced inhibition is preserved in the presence of a large (1,000 μm) mask and is blocked by TTX. This is consistent with the extensive axon-like and action potential–generating processes of polyaxonal cells. Saturation of inhibition with increasing area is consistent with the measured tracer coupling among the dendrites of polyaxonal cells. The broad tuning of the shift inhibition coincides with the lack of surround inhibition in the ON-OFF polyaxonal cells[36]. The dendrites of all suppressed cells ramify within a central band in the IPL bounded by the directionally selective ganglion cell dendrites, the same regions where the ON-OFF polyaxonal cell processes ramify. Finally, inhibition is mediated by GABA, the transmitter localized[41] in polyaxonal cells. This suggests that polyaxonal cells mediate fast shift inhibition, although other less well characterized axon-bearing amacrine cells, which costratify with the suppressed cells, could also be involved.

It is important to note that the windmill-evoked inhibition in salamanders has different functional properties from the shift-evoked inhibition measured here: in salamanders, sustained windmill motion effectively evokes inhibition, and a very slowly spinning windmill (0.03 rev/s, 0.1 mm/s on the retina) was able to fully activate the inhibition[24]. The magnitude of inhibition fell almost to zero at higher velocities (1 rev/s). The global shift–evoked fast inhibition reported here was silent during sustained image shift and was not activated at lower speeds (**Fig. 1d,e**). Moreover, the inhibition in salamander is glycinergic[21]; the one measured here is GABAergic.

In the cat retina, a moving pattern evoked inhibition that was delayed[23] by 100 ms compared to the center response of the measured ganglion cell. A possible explanation for the difference between our study and that study is that the fast inhibition in our experiments was evoked by either scene cuts or rapid (100–150 °/s) shifts. The speed of the moving pattern was an order of magnitude lower (2 °/s) in the cat study.

Our results indicate an extraordinary level of refinement and specificity of neural connections in the mammalian inner retina. They identify, on a layer-by-layer basis, the specific retinal cell types that are suppressed by abrupt shifts in natural scenes, and those that are not. This study suggests that specific ganglion cell types will be suppressed during saccadic eye movements[42] in rabbits.

The primate retina also contains axon-bearing amacrine cells with similar layering and functional properties as the rabbit polyaxonal cells[39,40]. Moreover, primate parasol cells, which give rise to the magnocellular outflow of the retina, costratify[43] with the axonal plexus of the axon-bearing amacrine cells. That is consistent with the psychophysical finding that saccadic suppression primarily affects the magnocellular pathway[44]. It is not clear, however, whether any rabbit cell type corresponds to the parvocellular outflow of the primate retina, which is less affected[44] by saccadic suppression.

It is therefore conceivable that the reported suppression of activity in the lateral geniculate nucleus[45,46] and in V1[47], as well as the visual threshold elevation and 'negative time' phenomenon during visual shifts that simulate saccadic eye movements[48], are at least partly due the globally mediated fast inhibition in the retina described here. Other non-retinal mechanisms of saccadic suppression exist as well, as the suppression of phosphenes can occur in total darkness[49], and saccadic suppression can begin before an eye movement[26].

In summary, the retina not only generates a set of specific representations of the visual world, but also appears to parse their transmission to higher centers during rapid global shifts.

METHODS

Electrophysiology. All experiments were performed according to UC Berkeley institutional guidelines. We recorded from 130 ganglion cells in the visual streak of isolated, light-adapted whole-mount retinas of 2.5-kg New Zealand White rabbits using an Axopatch 200B amplifier (Axon Instruments). From each ganglion cell, we recorded with two electrodes. First we recorded spiking with a loose cell-attached electrode (resistance, 3–4 MΩ) filled with Ames solution. Second, we recorded inhibitory and excitatory currents with a whole-cell electrode (5–8 MΩ) filled with 113 mM $CsMeSO_4$, 1 mM Mg SO_4, 7.8 10^{-3} mM $CaCl_2$, 0.1 mM BABTA, 10 mM HEPES, 4 mM ATP-Na_2, 0.5 mM GTP-Na_3, 5 mM QX314-Br, 7.5 mM Neurobiotin-Cl, pH 7.2. The retina was continuously perfused at 8–10 ml/min with Ames (pH 7.4) solution at 36 °C, equilibrated with 95% O_2 and 5% CO_2. Under these conditions, the isolated rabbit retina preserved its light response for 6–7 h (we have not tested longer periods of time). Excitatory currents were measured by clamping cells to an E_{Cl} of –60 mV. Inhibitory currents were measured by clamping the membrane to 0 mV, the reversal potential for ionotropic glutamate receptors. The recorded currents in voltage clamp are measures of the change in inhibitory or excitatory conductance. For further details, see **Supplementary Methods** online and ref. 6. QX314 was used to block sodium currents internally. The data acquisition software, RED, was written by M. Wang, E. Nemeth, D. Handwerker and T. Lan in our laboratory. Data were analyzed in Mathematica (Wolfram Research).

Confocal reconstruction. Confocal reconstruction of ganglion cells was done on a MRC 1024 (Bio-Rad Laboratories) or LSM 510 (Zeiss) confocal microscope as described previously[1]. Briefly, cells were loaded with neurobiotin, fixed, and incubated with streptavidin-Alexa Fluor 488 conjugate to stain the measured cell and ToPro3 to stain all cell nuclei. We mounted all retinas with Pro-Long antifade kit (Molecular Probes).

Light stimulus. An LCD panel, illuminated by a variable-intensity (0–2,000 W) spatially homogenous lamp, projected the stimulus videos onto the photoreceptor layer of the light-adapted whole-mount rabbit retina as described previously[6]. The time constant of the LCD panel was 12 ms. The contrast was defined as $(I - I_{background})/I_{background}$, where I is the intensity of light measured at the place of the retina. $I_{background}$ is the background intensity measured at the place of the retina that corresponds to grayscale value 128 of the LCD panel. The grayscale value-to-contrast function was measured to be $-90 + 640/(1 + 41 \exp[0.015(248 - x)])$.

Videos were acquired with a digital video recorder (Sony, DCR-TRV125E). The videos were displayed as a 30 frame/s bitmap (400 × 400 BMP) sequence by Presentation (NBS) software driven from RED. The same video was presented at 11 or 21 different locations separated by 50 or100 μm in a row. The video covered a 2 × 2 mm or 4 × 4 mm area on the retina (1 pixel = 5 μm or 10 μm). Before each video presentation, a 100-μm spot was flashed at the receptive field center of the ganglion cell to assure that its response properties did not change during the separate video presentations. The ganglion cell body was at the center of the 6th of the 11 presentations.

The local illumination waveform was measured at the LCD panel with a photodiode in an area that corresponded to a 200-μm diameter spot at the center of the measured cell. In **Fig. 2e**, we stimulated the measured ganglion cell with spots of different sizes (50–2,000 μm diameter) and showed the fastest excitatory current (blue) as well as the inhibitory response (red) to a large (1,000–2,000 μm) spot. In **Fig. 4b**, the checkerboard flicker was presented outside of a 1,000-μm mask for 100 ms (three frames). The temporal frequency of the flicker was 30 frames/s; the squares in the checkerboard were black and white and changed polarity in each frame. In the experiment shown in **Fig. 4c**, we presented a 2,000 × 500 μm checkerboard flicker stripe at different distances from the measured cell for 100 ms. The square size was 100 μm. For the experiments shown in **Fig. 5a**, a subregion was defined as 1/16 of a ring (700 μm inner, 2,000 μm outer diameter). A subregion stimulation was defined as a 100-ms flicker of a 100-μm checkerboard in the subregion. For the simultaneous subregion stimulation experiments, we used two different stimulation sequences: we either stimulated more and more subregions counterclockwise in a linear order, or we sequentially stimulated subregions that were the farthest apart.

Design of scene shifts. Shifts in the video were designed to approximate the speed and amplitude of saccadic shifts in the rabbit[42]. In freely moving rabbits, the modal, median and mean saccadic amplitudes are 10°, 19° and 20°, respectively. The maximum saccadic speed (V_{max}) is linearly dependent on the amplitude by the following function: $V_{max}(°/s) = 128 + 11.4A$, where A is the saccadic amplitude. In rabbits, 170 μm of retinal distance is equivalent to1° in visual space[50]. A shift in the video was recorded by rapidly manually pointing the camera to a new location. The recorded videos were analyzed in Mathematica (Wolfram Research), and ten videos were chosen from many video recordings that had shift amplitudes and velocities in the range measured in rabbits. The saccadic amplitudes in this study (10–20°) were similar to that used in primates (20°) previously[47]. The shifts lasted 2–3 frames (66–99 ms). One video (III) was created digitally in Mathematica from a photograph by scanning horizontally through the picture. A scene cut was introduced into video II by cutting together two recorded videos. The different videos lasted 2–8 s and contained 1–2 shifts. The quantification of the video parameters is shown in **Supplementary Fig. 1**. Eleven different videos with rapid global shifts are labeled with roman numbers in the figures. Video I may be seen online (**Supplementary Video**) and videos II–XII can be viewed at http://mcb.berkeley.edu/labs/werblin/.

Cell classification. It was based on measurements from more than 320 cells. Types 1–10 were defined previously[6]. Types 11–13 were added here. The G1–11 classification was based on ref. 10.

Note: Supplementary information is available on the Nature Neuroscience website.

ACKNOWLEDGMENTS

We thank D. Takacs and M. Jaszberenyi for their technical assistance, D. Balya for his comments on the experiments and R. Zucker for his comments on the manuscript. This study was supported by the Office of Naval Research.

COMPETING INTERESTS STATEMENT

The authors declare that they have no competing financial interests.

Received 17 February; accepted 28 April 2003
Published online 12 May 2003; doi:10.1038/nn1061

1. Boycott, B. & Wassle, H. Morphological classification of bipolar cells of the primate retina. *Eur. J. Neurosci.* **3**, 1069–1088 (1991).
2. Euler, T. & Wassle, H. Immunocytochemical identification of cone bipolar cells in the rat retina. *J. Comp. Neurol.* **361**, 461–478 (1995).
3. McGillem, G.S. & Dacheux, R.F. Rabbit cone bipolar cells: correlation of their morphologies with whole-cell recordings. *Vis. Neurosci.* **18**, 675–685 (2001).
4. Wu, S.M., Gao, F. & Maple, B.R. Functional architecture of synapses in the inner retina: segregation of visual signals by stratification of bipolar cell axon terminals. *J. Neurosci.* **20**, 4462–4470 (2000).
5. MacNeil, M.A., Heussy, J.K., Dacheux, R.F., Raviola, E. & Masland, R.H. The shapes and numbers of amacrine cells: matching of photofilled with Golgi-stained cells in the rabbit retina and comparison with other mammalian species. *J. Comp. Neurol.* **413**, 305–326 (1999).
6. Roska, B. & Werblin, F. Vertical interactions across ten parallel, stacked representations in the mammalian retina. *Nature* **410**, 583–587 (2001).
7. Boycott, B. & Wässle, H. Parallel processing in the mammalian retina: the Proctor Lecture. *Invest. Opthal. Vis. Sci.* **40**, 1313–1327 (1999).
8. Masland, R.H. The fundamental plan of the retina. *Nat. Neurosci.* **4**, 877–886 (2001).
9. O'Brien, B.J., Isayama, T., Richardson, R. & Berson, D.M. Intrinsic physiological properties of cat retinal ganglion cells. *J. Physiol.* **538**, 787–802 (2002).
10. Rockhill, R.L., Daly, F.J., MacNeil, M.A., Brown, S.P. & Masland, R.H. The diversity of ganglion cells a mammalian retina. *J. Neurosci.* **22**, 3831–3843 (2002).
11. Devries, S.H. & Baylor, D.A. Mosaic arrangement of ganglion cell receptive fields in rabbit retina. *J. Neurophysiol.* **78**, 2048–2060 (1997).
12. Sun, W., Li, N. & He, S. Large-scale morphological survey of mouse retinal ganglion cells. *J. Comp. Neurol.* **451**, 115–126 (2002).
13 Huxlin, K.R. & Goodchild, A.K. Retinal ganglion cells in the albino rat: revised morphological classification. *J. Comp. Neurol.* **385**, 309–323 (1997).
14. Kolb, H., Linberg, K.A. & Fisher, S.K. Neurons of the human retina: a Golgi study. *J. Comp. Neurol.* **318**, 147–187 (1992).
15. Dacey, D.M., Peterson, B.B., Robinson, F.R. & Gamlin, P.D. Fireworks in the primate retina. *In vitro* photodynamics reveals diverse LGN-projecting ganglion cell types. *Neuron* **37**, 15–27 (2003).
16. Mangrum, W.I., Dowling, J.E. & Cohen, E.D. A morphological classification of ganglion cells in the zebrafish retina. *Vis. Neurosci.* **19**, 767–779 (2002).
17. Arkin, M.S. & Miller, R.F. Mudpuppy retinal ganglion cell morphology revealed by an HRP impregnation technique which provides Golgi-like staining. *J. Comp. Neurol.* **270**, 185–208 (1988).
18. Kock, J.H. *et al.* Ganglion cells in the frog retina: discriminant analysis of histological classes. *Vision Res.* **29**, 1–18 (1989).
19. Cohen, E.D. Interactions of inhibition and excitation in the light-evoked currents of X-type retinal ganglion cells. *J. Neurophysiol.* **80**, 2975–2990 (1998).
20. Werblin, F.S. Lateral interactions at inner plexiform layer of vertebrate retina: antagonistic responses to change. *Science* **175**, 1008–1010 (1972).
21. Cook, P.B., Lukasiewicz, P.D. & McReynolds, J.S. Action potentials are required for the lateral transmission of glycinergic transient inhibition in the amphibian retina. *J. Neurosci.* **18**, 2301–2308 (1998).
22. Demb, J.B., Haarsma, L., Freed, M.A. & Sterling, P. Functional circuitry of the retinal ganglion cell's nonlinear receptive field. *J. Neurosci.* **19**, 9756–9767 (1999).
23. Enroth-Cugell, C. & Jakiela, H.G. Suppression of cat retinal ganglion cell responses by moving patterns. *J. Physiol.* **302**, 49–72 (1980).
24. Thibos, L.N. & Werblin, F.S. The properties of surround antagonism elicited by spinning windmill patterns in the mudpuppy retina. *J. Physiol.* **278**, 101–116 (1978).
25. Werblin, F.S. & Copenhagen, D.R. Control of retinal sensitivity. Lateral interactions at the inner plexiform layer. *J. Gen. Physiol.* **63**, 88–110 (1974).
26. Ross, J., Morrone, M.C., Goldberg, M.E. & Burr, D.C. Changes in visual perception at the time of saccades. *Trends Neurosci.* **24**, 113–121 (2001).
27. McIlwain, J.T. Some evidence concerning the physiological basis of the periphery effect in the cat's retina. *Exp. Brain Res.* **1**, 265–271 (1966).
28. Barlow, H.B., Derrington, A.M., Harris, L.R. & Lennie, P. The effects of remote retinal stimulation on the responses of cat retinal ganglion cells. *J. Physiol.* **269**, 177–194 (1977).
29. Brivanlou, I.H., Warland, D.K. & Meister, M. Mechanisms of concerted firing among retinal ganglion cells. *Neuron* **20**, 527–539 (1998).
30. Fischer, B., Kruger, J. & Droll, W. Quantitative aspects of the shift-effect in cat retinal ganglion cells. *Brain Res.* **83**, 391–403 (1975).
31. Noda, H. & Adey, W.R. Retinal ganglion cells of the cat transfer information on saccadic eye movement and quick target motion. *Brain Res.* **70**, 340–345 (1974).
32. Taylor, W.R. TTX attenuates surround inhibition in rabbit retinal ganglion cells. *Vis. Neurosci.* **16**, 285–290 (1999).
33. Flores-Herr, N., Protti, D.A. & Wassle, H. Synaptic currents generating the inhibitory surround of ganglion cells in the mammalian retina. *J. Neurosci.* **21**, 4852–4863 (2001).
34. Menger, N., Pow, D.V. & Wässle, H. Glycinergic amacrine cells of the rat retina. *J. Comp. Neurol.* **401**, 34–46 (1998).
35. Feigenspan, A., Wässle, H. & Bormann, J. Pharmacology of GABA receptor Cl- channels in rat retinal bipolar cells. *Nature* **361**, 159–162 (1993).
36. Völgyi, B., Xin, D., Amarillo, Y. & Bloomfield, S.A. Morphology and physiology of the polyaxonal amacrine cells in the rabbit retina. *J. Comp. Neurol.* **440**, 109–125 (2001).
37. Famiglietti, E.V. Polyaxonal amacrine cells of rabbit retina: morphology and stratification of PA1cells. *J. Comp. Neurol.* **316**, 391–405 (1992).
38. Vaney, D.I., Peichl, L. & Boycott, B.B. Neurofibrillar long-range amacrine cells in mammalian retinae. *Proc. R. Soc. Lond. B Biol. Sci.* **235**, 203–219 (1988).
39. Dacey, D.M. Axon-bearing amacrine cells of the macaque monkey retina. *J. Comp. Neurol.* **284**, 275–293 (1989).
40. Stafford, D.K. & Dacey, D.M. Physiology of the A1 amacrine: a spiking, axon-bearing interneuron of the macaque monkey retina. *Vis. Neurosci.* **14**, 507–522 (1997).
41. Pourcho, R.G. & Goebel, D.J. Neuronal subpopulations in cat retina which accumulate the GABA agonist (3H) muscimol: a combined Golgi and autoradiographic study. *J. Comp. Neurol.* **219**, 25–35 (1983).
42. Collewijn, H. Eye and head movements in freely moving rabbits. *J. Physiol.* **266**, 471–498 (1977).
43. Watanabe, M. & Rodieck, R.W. Parasol and midget ganglion cells of the primate retina. *J. Comp. Neurol.* **289**, 434–454 (1989).
44. Burr, D.C., Morrone, M.C. & Ross, J. Selective suppression of the magnocellular visual pathway during saccadic eye movements. *Nature* **371**, 511–513 (1994).
45. Noda, H. Depression of the excitability of relay cells of lateral geniculate nucleus following saccadic eye movements in the cat. *J. Physiol.* **249**, 87–102 (1975).
46. Reppas, J.B., Usrey, W.M. & Reid, R.C. Saccadic eye movements modulate visual responses in the lateral geniculate nucleus. *Neuron* **35**, 961–974 (2002).
47. Wurtz, R.H. Comparison of effects of eye movements and stimulus movements on striate cortex neurons of the monkey. *J. Neurophysiol.* **32**, 987–994 (1969).
48. Mackay, D.M. Elevation of visual threshold by displacement of retinal image. *Nature* **225**, 90–92 (1970).
49. Riggs, L.A., Merton, P.A. & Morton, H.B. Suppression of visual phosphenes during saccadic eye movements. *Vision Res.* **14**, 997–1011 (1974).
50. Hughes, A. Topographical relationships between the anatomy and physiology of the rabbit visual system. *Doc. Ophthalmol.* **30**, 33–159 (1971).